The Astrophysical Journal Letters, 874:L7 (5pp), 2019 March 20 https://doi.org/10.3847/2041-8213/ab0c10


# A GeV–TeV Measurement of the Extragalactic Background Light

A. Desai[1], K. Helgason[2], M. Ajello[1], V. Paliya[3], A. Domínguez[4], J. Finke[5], and D. Hartmann[1]
[1] Department of Physics and Astronomy, Clemson University, Kinard Lab of Physics, Clemson, SC 29634-0978, USA; abhishd@g.clemson.edu
[2] Science Institute, University of Iceland, IS-107 Reykjavik, Iceland; helgason@hi.is
[3] Deutsches Elektronen Synchrotron DESY, Platanenallee 6, D-15738 Zeuthen, Germany
[4] Grupo de Altas Energías, Universidad Complutense de Madrid, E-28040 Madrid, Spain
[5] Space Science Division, Naval Research Laboratory, Washington, DC 20375-5352, USA
*Received 2019 January 15; revised 2019 February 26; accepted 2019 February 27; published 2019 March 22*

## Abstract

The extragalactic background light (EBL) can be probed via the absorption imprint it leaves in the spectra of gamma-ray sources ($\gamma\gamma \rightarrow e^{-}e^{+}$). We recently developed a dedicated technique to reconstruct the EBL, and its evolution with redshift, from $\gamma$-ray optical depth data using a large sample of blazars detected by the *Fermi* Large Area Telescope. Here, we extend this data set to the TeV regime using ground-based Cherenkov observations of 38 blazars and report the first homogeneous measurement of the EBL spectral intensity covering the ultraviolet to infrared wavelengths ($\sim$0.1–100 $\mu$m). A minimal EBL throughout the wavelength range with respect to integrated galaxy light is found, allowing little additional unresolved emission from faint or truly diffuse populations setting an upper limit of $\lesssim$4 nW m$^{-2}$ sr$^{-1}$ at 1.4 $\mu$m. In particular, the cosmic optical background at $z = 0$ is found to be $27.8^{+2.1}_{-2.0}$ nW m$^{-2}$ sr$^{-1}$. This work lays the foundation for accurate gamma-ray measurements of the EBL across its whole spectral range using a combination of GeV and TeV data.

*Key words:* BL Lacertae objects: general – cosmic background radiation – gamma rays: general

## 1. Introduction

The extragalactic background light (EBL) is the diffuse background radiation accumulated over the cosmic history at ultraviolet (UV), optical, and infrared (IR) wavelengths (e.g., Dwek & Krennrich 2013). The local EBL energy spectrum comprises two peaks, with the first peak ($\approx$1 $\mu$m) due to direct emission from stars and the second peak ($\approx$100 $\mu$m) due to reprocessed starlight emission by dust within galaxies (Brun 2013). Measurements of both the EBL spectral intensity and its evolution are important to study both star formation and galaxy evolution processes (e.g., Raue & Meyer 2012; Cowley et al. 2018; Khaire & Srianand 2018).

Measuring the EBL brightness has proven challenging mainly due to bright foreground contaminants such as the zodiacal light and the diffuse galactic light (Hauser et al. 1998). Studying the signatures left by the EBL in the spectra of distant $\gamma$-ray sources, via the photon–photon interaction, is emerging as the most powerful technique to probe the EBL. Various attempts have been made to constrain the EBL intensity using the absorption found in the spectrum of blazars at 0.1–100 GeV high energy and 0.1–30 TeV very high energy (VHE). The constraints came first in the form of upper limits on the intensity (e.g., Aharonian et al. 2006; Mazin & Raue 2007; Meyer et al. 2012) and later as measurements of the actual levels (e.g., Ackermann et al. 2012; Abramowski et al. 2013; Biteau & Williams 2015; Ahnen et al. 2016). However, the majority of the above measurements rely on scaling existing EBL models (like the models of Kneiske & Dole 2010; Finke et al. 2010; Domínguez et al. 2011; Gilmore et al. 2012; Stecker et al. 2016; etc.) in amplitude. To improve this, we have developed a method to reconstruct the EBL spectrum and evolution based on measured $\gamma$-ray optical depths (see The Fermi-LAT Collaboration 2018).

In this Letter, we apply this newly developed tool to measure the EBL using both GeV and TeV data. While the GeV optical depths are taken from The Fermi-LAT Collaboration (2018), the TeV optical depths are derived using the multiple spectra of 38 TeV blazars reported in Biteau & Williams (2015). The combined data set enables us to consistently constrain the EBL spectral intensity in the wavelength regime 0.1 to 100 $\mu$m. The paper is organized as follows: in Section 2 we describe the procedure used to derive the TeV optical depths, in Section 3 we describe the methodology used to reconstruct the EBL, and in Section 4 we discuss the implications of our measurements.

## 2. Analysis

### 2.1. The Intrinsic Blazars' Spectra

Our analysis relies on the 106 VHE gamma-ray spectral energy distributions (SEDs) of 38 blazars reported in Biteau & Williams (2015). The source photons in this sample originate from $z = 0.019$ to $z = 0.604$ and are detected in the 0.1–21 TeV range. The SEDs are modeled in this energy range using:

$$\frac{dN}{dE}_{\rm obs} = \frac{dN}{dE}_{\rm int} \cdot e^{-b\cdot\tau_{\rm model}}, \quad (1)$$

where $dN/dE_{\rm int}$ and $dN/dE_{\rm obs}$ are the intrinsic and observed blazar spectrum, respectively, $\tau_{\rm model}(E)$ is the optical depth estimated by EBL models at the source redshift (e.g., Finke et al. 2010; Kneiske & Dole 2010; Domínguez et al. 2011; Gilmore et al. 2012) and $b$ is a renormalization constant to scale the optical depth.

To model the intrinsic spectrum we follow the methodology similar to previous analyses of VHE data where four different intrinsic spectral functions are used (see also Biteau & Williams 2015; Magic Collaboration 2019). These models are power law, log-parabola, power law with exponential cutoff, and log-parabola with exponential cutoff. For a given EBL model (see, e.g., Table 1), the intrinsic spectrum of a source is then chosen by adopting the function that produces the highest $\chi^2$ probability when $b = 1$.

For a given EBL model and for each source, a likelihood profile of the renormalization constant $b$ is produced. This is

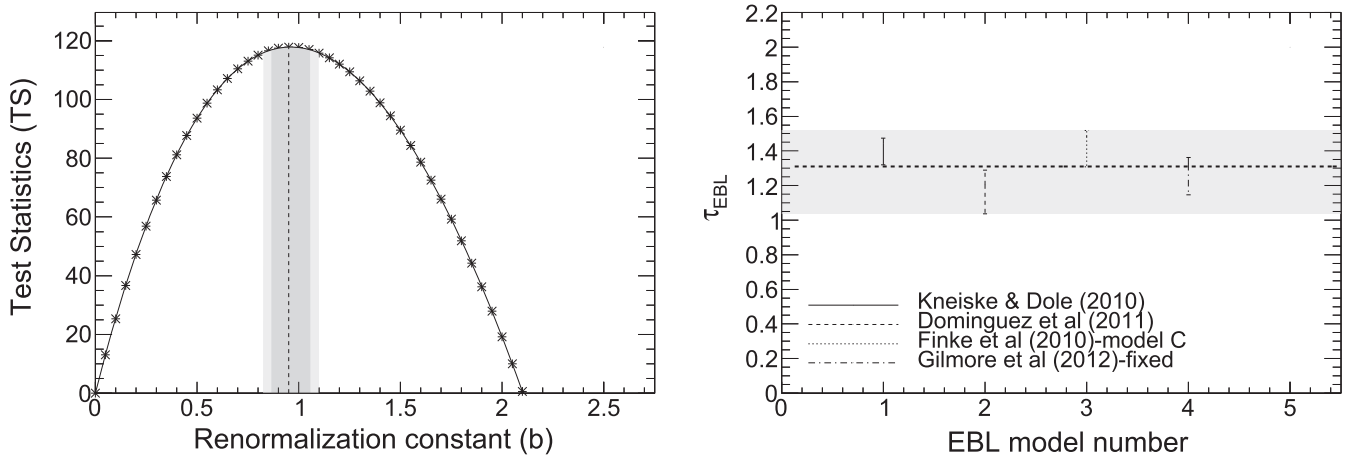


**Figure 1.** Left: stacked TS profile obtained for a range of $b$ values using the EBL optical depths given by Biteau & Williams (2015). The dotted line shows the best-fit value of $b$ for the given EBL model. The shaded dark gray region highlights the $1\sigma$ contour while the light gray region shows the $2\sigma$ contour. Right: example of how the optical depth is derived for a given energy and redshift bin using the values of $\tau$ derived using four different EBL models. The horizontal dashed line shows the best-fit value of the optical depth, while its uncertainty (the gray band) is chosen to encompass the uncertainty of all models.

**Table 1**
Results of EBL Models Tested using VHE Data

| Model | $b_{\text{best-fit}}$[a] | Test Statistic[b] |
|---|---|---|
| Finke et al. (2010)—model C | $1.05^{-0.15}_{+0.12}$ | 71.60 |
| Kneiske & Dole (2010) | $1.4^{-0.16}_{+0.14}$ | 99.47 |
| Domínguez et al. (2011) | $0.85^{-0.10}_{+0.08}$ | 105.98 |
| Gilmore et al. (2012)—fixed | $1.00^{-0.16}_{+0.12}$ | 106.13 |
| Biteau & Williams (2015) | $0.95^{-0.08}_{+0.11}$ | 117.83 |

**Notes.**
[a] Best-fit renormalization constant derived from the stacking analysis.
[b] TS obtained by comparing the log likelihood obtained for the null case of $b = 0$ with the value obtained for $b = b_{\text{best-fit}}$.

transformed into a test statistic (TS) profile, by subtracting the value of the log likelihood at $b = 0$ and multiplying by two. For a given EBL model, the TS profiles of all sources are summed generating a "stacked" TS, which allows us to identify the best-fit value of $b$ for all spectra. This stacked TS value also displays the significance of the result as $\sqrt{\text{TS}}$ (see also Ackermann et al. 2012; Abramowski et al. 2013; Desai et al. 2017). The stacked TS versus $b$ profile for one EBL model is shown in Figure 1. There is a maximum TS of 117.83, which implies a detection at approximately $10.85\sigma$. Table 1 shows the results obtained using five different EBL models.

### 2.2. Deriving the EBL Optical Depths

In order to measure the optical depth, we perform a stacking analysis where the source sample is divided into two redshift bins and the analysis is performed across four energy bins. While the two redshift bins ($0.01 < z < 0.04$ and $0.04 < z < 0.604$) are chosen such that they contain the same signal strength (TS contribution to the analysis described in Section 2.1), the energy bins are chosen to have equal logarithmic widths. For each energy and redshift bin, a stacked TS versus $b$ profile is derived using the method described in Section 2.1 where the source sample and energy range is modified according to the bin being considered. The corresponding $b$ value, in each redshift and energy bin, is then used alongside the EBL model being tested to obtain the optical depth (as obtained using that model).

We perform the above binned analysis for four[6] different EBL models (Finke et al. 2010; Kneiske & Dole 2010; Domínguez et al. 2011; Gilmore et al. 2012). In a given energy and redshift bin, the optical depth is derived as the mean of the four individual optical depth measurements (derived using four different EBL models), while the uncertainty is chosen as the one that encompasses the uncertainties of all the optical depth measurements, as shown in Figure 1. Along with the statistical uncertainties, the uncertainty on the optical depth includes a systematic contribution due to the difference in shape of the optical depth curve estimated from EBL models, the intrinsic model used in Equation (1) and the systematic energy bias of $\approx$10% found in TeV data measured using Cherenkov telescopes (Meyer et al. 2010). As in Biteau & Williams (2015), the impact of these systematic uncertainties on the EBL optical depth is estimated to be $\approx$2%–5%. We include these uncertainties in our measurement of the derived optical depth values and show it in Figure 2. These optical depth measurements are also made available in an online database.[7]

## 3. Reconstructing the EBL

We use the derived optical depths to reconstruct the absorbing EBL in a model independent way. In what follows, we include optical depth measurements at $\lesssim$1 TeV by The Fermi-LAT Collaboration (2018) based on a sample of 739 blazars observed by the *Fermi*-Large Area Telescope (LAT). These measurements provide $\tau(E, z)$ in 12 redshift bins in the $z = 0.03$–$3.1$ range and are thus highly complementary to our VHE data set. Whereas the optical depths at VHE constrain the local EBL from optical to far-IR wavelengths, the *Fermi*-LAT data set probes the UV to optical out to high redshifts. In terms of wavelength and redshift coverage, the combined data set results in the most extensive constraints of the EBL to date.

We follow the novel methodology presented by The Fermi-LAT Collaboration (2018), where the cosmic emissivity (luminosity density) is modeled as the sum of several log-

[6] The optical depths reported in Biteau & Williams (2015) were optimized relying on the data used in this work and as such are not used here.
[7] https://figshare.com/s/9cd4f26925945470582a

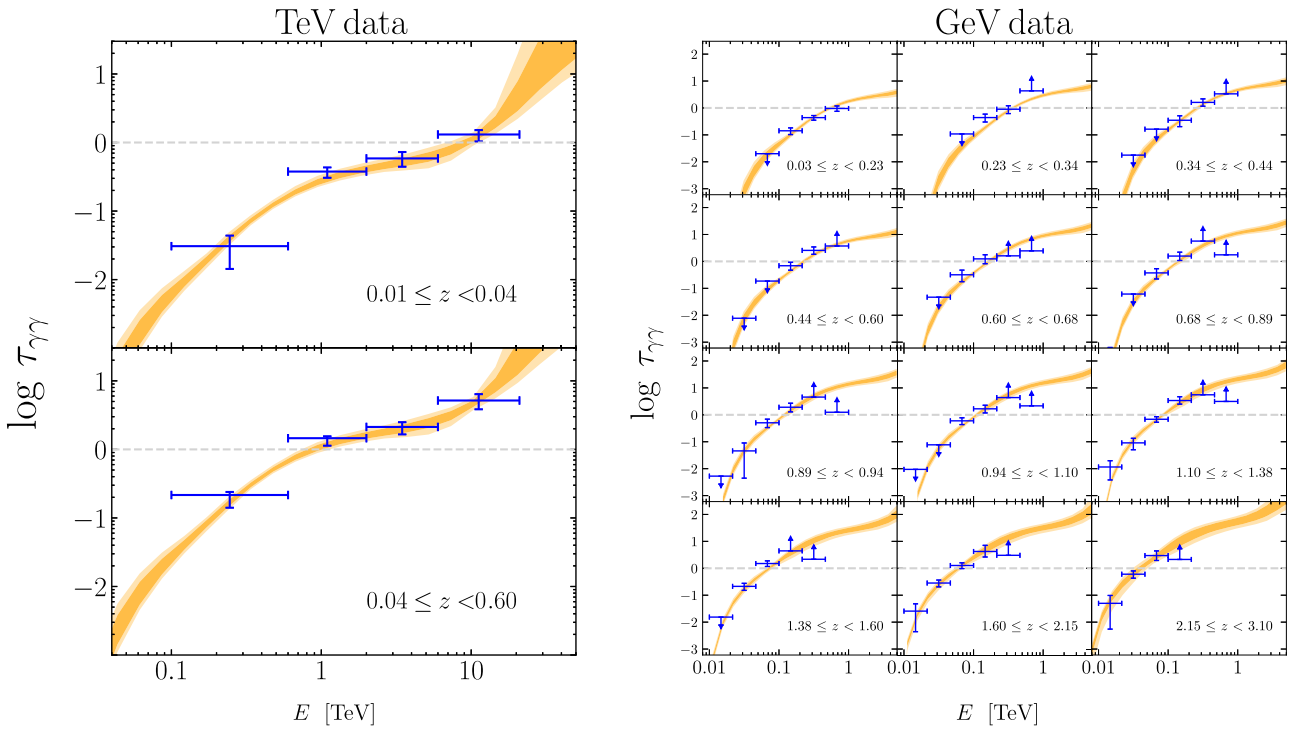


**Figure 2.** Redshift binned optical depth measurements derived from the stacking analysis using VHE data (left) and *Fermi*-LAT data (right) are shown compared to the optical depth templates reported by this work. The shaded regions signify the $1\sigma$ and $2\sigma$ confidence regions of our best-fitting EBL reconstruction.

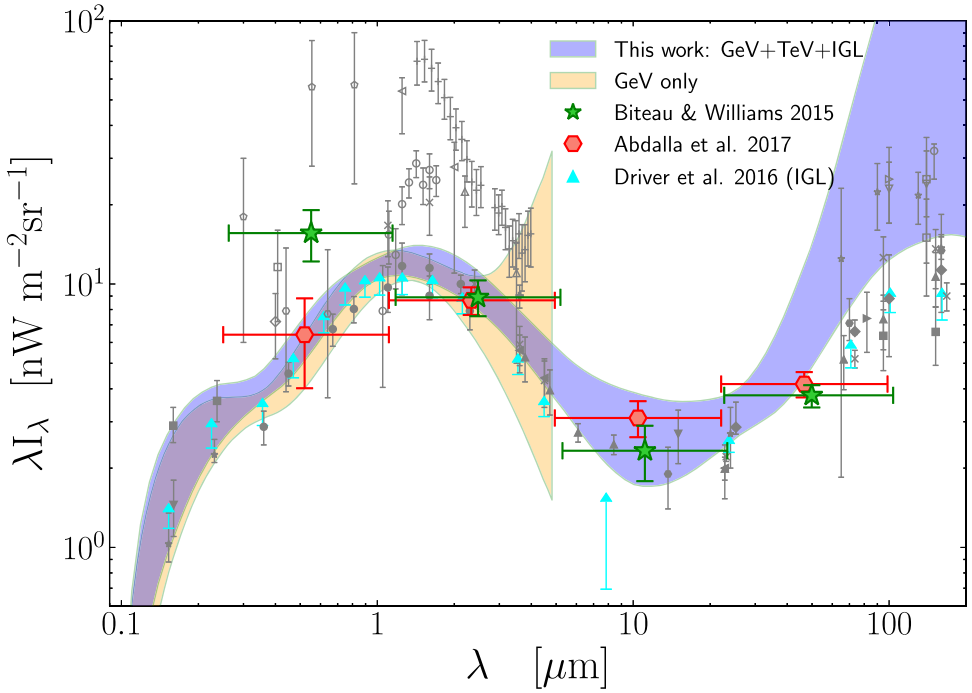


**Figure 3.** Spectral intensity of the EBL from UV to far-IR. The constraints from this work are shown as a 68% confidence region and median (blue). A corresponding region from The Fermi-LAT Collaboration (2018) that relies on GeV data only is shown in orange. Various measurements in the literature are shown in gray: direct measurements (open symbols), integrated galaxy counts (filled symbols). The numerical data of the blue and orange curves are available at https://figshare.com/s/9cd4f26925945470582a.

normal templates with a fixed peak position

$$j(\lambda) = \sum_i a_i \cdot \exp\left[-\frac{(\log\lambda - \log\lambda_i)^2}{2\sigma^2}\right] \quad (2)$$

in erg s$^{-1}$ cm$^{-3}$ Å$^{-1}$, where the pivots are logarithmically spaced with $\Delta_{\lg\lambda} = 0.5$, resulting in seven templates centered at $\lambda_i = [0.16, 0.50, 1.6, 5.0, 16, 50, 160]$ $\mu$m. We fix $\sigma = 0.2$, and leave the amplitudes $a_i$ free to vary. We tried varying the number of templates and their placement under the condition that $\sigma = \Delta_{\lg\lambda}/2.5$ and find that the local EBL is always consistent within the $1\sigma$ confidence region of the final result shown in Figure 3. Each template is allowed to evolve

independently with redshift according to

$$j(\lambda_i, z) = j_0(\lambda_i) \cdot \begin{cases} \frac{(1+z)^{b_i}}{1+\left(\frac{1+z}{c_i}\right)^{d_i}}, & i \leqslant 3 \\ (1+z)^{b_i}, & i > 3, \end{cases} \quad (3)$$

where $j_0(\lambda_i) \equiv j(\lambda_i, z = 0)$ is the emissivity at the present time centered at $\lambda_i$. We reduce the number of parameters by splitting the evolution form at $\lambda \simeq 5\ \mu$m as the TeV sources are only sensitive to EBL photons at low-$z$ toward IR wavelengths. This results in 18 free parameters.

The local EBL is obtained from the evolving emissivity $j(\lambda, z)$:

$$\lambda I_\lambda = \frac{c}{4\pi} \int \lambda' j(\lambda', z) \frac{dt}{dz} \frac{dz}{(1+z)}, \quad (4)$$

where $\lambda' = \lambda/(1+z)$ is the rest-frame wavelength.

The MCMC code `emcee` (Foreman-Mackey et al. 2013), a Python implementation of an affine invariant MCMC ensemble sampler (Goodman & Weare 2010), is used to constrain the parameters controlling the emissivity. With the emissivity specified as a function of wavelength and redshift, we calculate the resulting EBL and optical depth at 14 redshifts corresponding to each of the bins in Figure 2. In addition to the optical depth data, we have included the integrated galaxy counts from Driver et al. (2016) as lower limits on the EBL at $z = 0$. These are taken to be the lower uncertainty for the galaxy light data obtained by integrating over the observed magnitude range only, i.e., not extrapolated.[8] The likelihood function is estimated as $\mathcal{L} \propto \exp(-\chi^2)$ where the total number of optical depth data points and EBL lower limits used to calculate $\chi^2$ is 97. Our final results are based on MCMC chains from 120 walkers exploring the parameter space in 10,000 steps each. This results in 1,140,000 steps after a burn-in of 500 steps for each walker. We refer to The Fermi-LAT Collaboration (2018) for details.

## 4. Discussion

The measured constraints on the local EBL with a 68% confidence region are displayed in Figure 3. For a comparison, we also show previous measurements reported in the literature. While the results are in good agreement with the *Fermi*-LAT measurement (orange) relying on GeV data only (The Fermi-LAT Collaboration 2018), a minor difference is seen in the higher end of the uncertainty at $\approx 2\ \mu$m, which is mainly driven by the Cherenkov measurements of the repeatedly observed Mkn 421 and Mkn 501.

The slightly larger-intensity of the GeV+TeV+IGL result, as compared to GeV only, is not entirely due to the inclusion of the IGL lower limits. In fact, examining the reduced $\chi^2 = \chi^2_{\rm GeV+TeV} + \chi^2_{\rm IGL}$ shows that the GeV+TeV data set prefers this intensity independently of the IGL lower limits. In other words, lowering the EBL intensity does not improve $\chi^2_{\rm GeV+TeV}$. This is also reflected in the reconstructed optical depths shown in Figure 2 that do not show systematically higher optical depths with respect to the data. However, we find that the IGL lower limits help constrain the spectral shape of the EBL, making the result less dependent on the placement of the spectral templates ($\lambda_i$). This is not surprising because the optical depth at a given energy is an integral over the EBL wavelengths encompassed by the photon–photon interaction cross-section.

An overall agreement is found with independent EBL measurements, both integrated galaxy counts and other $\gamma$-ray absorption studies. The combined GeV+TeV data set is also sensitive to EBL photons in the mid-IR ($\lesssim 100\ \mu$m), where we find good agreement with previous studies (Biteau & Williams 2015; Driver et al. 2016; H.E.S.S. Collaboration et al. 2017). However, the $\gamma$-ray data set has no constraining power at $\gtrsim 100\ \mu$m and the lower limits therefore push the EBL to higher far-IR values.

Our measurements are particularly valuable in the UV/optical, where previous $\gamma$-ray absorption studies had limited sensitivity, integrated counts show conflicting results (Gardner et al. 2000; Xu et al. 2005; Voyer et al. 2011) and direct measurements remain somewhat above the counts data (Bernstein 2007; Matsuoka et al. 2011; Mattila et al. 2017).

A key result of this work is a minimal EBL measurement throughout the wavelength range with respect to integrated galaxy light, allowing very little additional unresolved emission from faint or truly diffuse populations. We estimate the integrated cosmic background in the [0.09–8] $\mu$m range, often referred to as the cosmic optical background (COB), to be $27.8^{+2.1}_{-2.0}$ nW m$^{-2}$ sr$^{-1}$. We note that this is among the lowest estimates of the COB to date that is inferred from $\gamma$-ray data alone (see also Ahnen et al. 2016). At the reference wavelength of 1.4 $\mu$m we find $\lambda I_\lambda = 11.8^{+2.2(5.2)}_{-1.23(2.2)}$ nW m$^{-2}$ sr$^{-1}$ ($1\sigma(2\sigma)$), limiting any undetected contribution to the cosmic near-IR background to $\lesssim 4$ nW m$^{-2}$ sr$^{-1}$ ($1\sigma$) with respect to integrated counts of Driver et al. (2016), and even less with respect to Keenan et al. (2010). This suggests that larger values of the EBL inferred by direct measurements that rely on absolute flux calibration are not extragalactic and are likely attributable to Zodiacal light or other foreground emissions (Matsuura et al. 2017).

An important aspect of this work is the ability to constrain the build-up of the EBL with cosmic time. This is illustrated in Figure 4 where we measure that 50% of the COB has been accumulated by $z = 0.9$. The build-up of the EBL across the entire wavelength range is qualitatively consistent with that of state-of-the-art EBL models (Cowley et al. 2018).

The fact that the reconstructed EBL is remarkably similar to integrated counts data, and a host of existing models, suggests that significant systematic biases in our analysis are unlikely. Known systematic uncertainties are already included in the optical depth uncertainties. With nearly $\sim$800 blazars, any inaccuracies would need to affect the entire sample systematically in the same manner. Absorption intrinsic to the source (largely ruled out now by Costamante et al. 2018), for instance, from the black hole close environment or host galaxy, would result in the derived EBL being artificially larger, not lower. The fact that our EBL is already close to the minimum allowed by galaxy counts suggests that this effect, if present, is insignificant.

Finally, our work makes use of the latest blazar data from *Fermi*-LAT and present Cherenkov telescopes with a maximum energy of 21 TeV and allows us to constrain the EBL up to 70 $\mu$m. Long HAWC observations of bright blazars and observations by the upcoming CTA should be able to push this measurement even further, providing better IR constraints. At the same time, CTA should also be able to study the evolution

[8] We take the lower of the two PACS160 values given in Table 2 of Driver et al. (2016).

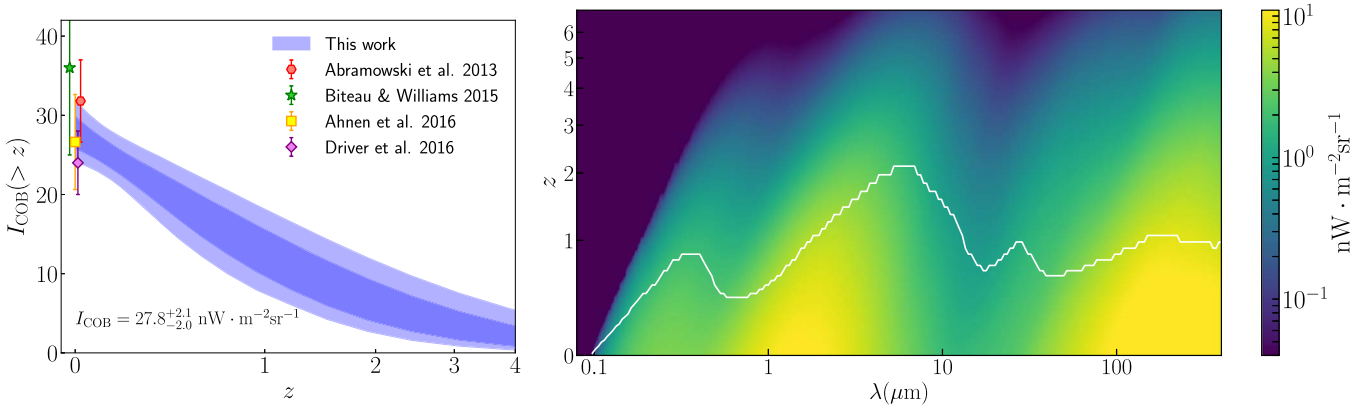


**Figure 4.** Build-up of the local EBL. The EBL at $z > 0$ is shown in comoving coordinates as a function of the observed wavelength. Left panel: the median and 68% confidence region of the build-up of the total background, integrated in the 0.1–8 $\mu$m range. Also displayed are $\gamma$-ray derived measurements of the COB at $z = 0$ from Abramowski et al. (2013), Biteau & Williams (2015), and Ahnen et al. (2016) and integrated counts from Driver et al. (2016). Right panel: the color map shows the median spectral intensity depicting the origin of the $z = 0$ EBL at a given wavelength. The white continuous line marks the redshift at which 50% of the local EBL has been accumulated. As the image shows the median EBL without uncertainties, we caution that the IR part is very poorly constrained, i.e., toward the upper right corner of the image.

of the EBL up to a redshift of 0.5 with 10% uncertainty (Gaté et al. 2017), effectively complementing our results.

A. Desai and M.A. acknowledge funding support from NSF through grant AST-1715256. K.H. acknowledges support from the Icelandic Research Fund, grant number 173728-051. The authors thank Dr. Biteau for providing the TeV spectra used in this work in a machine-readable format. A. Domínguez is thankful for the support of the Ramón y Cajal program from the Spanish MINECO.

## ORCID iDs

A. Desai https://orcid.org/0000-0001-7405-9994
K. Helgason https://orcid.org/0000-0002-4326-9144
M. Ajello https://orcid.org/0000-0002-6584-1703
V. Paliya https://orcid.org/0000-0001-7774-5308
A. Domínguez https://orcid.org/0000-0002-3433-4610
J. Finke https://orcid.org/0000-0001-5941-7933
D. Hartmann https://orcid.org/0000-0002-8028-0991

## References

Abramowski, A., Acero, F., Aharonian, F., et al. 2013, A&A, 550, A4
Ackermann, M., Ajello, M., Allafort, A., et al. 2012, Sci, 338, 1190
Aharonian, F., Akhperjanian, A. G., Bazer-Bachi, A. R., et al. 2006, Natur, 440, 1018
Ahnen, M. L., Ansoldi, S., Antonelli, L. A., et al. 2016, A&A, 590, A24
Bernstein, R. A. 2007, ApJ, 666, 663
Biteau, J., & Williams, D. A. 2015, ApJ, 812, 60
Brun, P. 2013, JPhCS, 460, 012015
Costamante, L., Cutini, S., Tosti, G., Antolini, E., & Tramacere, A. 2018, MNRAS, 477, 4749
Cowley, W. I., Lacey, C. G., Baugh, C. M., et al. 2018, MNRAS, submitted, (arXiv:1808.05208)
Desai, A., Ajello, M., Omodei, N., et al. 2017, ApJ, 850, 73
Domínguez, A., Primack, J. R., Rosario, D. J., et al. 2011, MNRAS, 410, 2556
Driver, S. P., Andrews, S. K., Davies, L. J., et al. 2016, ApJ, 827, 108
Dwek, E., & Krennrich, F. 2013, APh, 43, 112
Finke, J. D., Razzaque, S., & Dermer, C. D. 2010, ApJ, 712, 238
Foreman-Mackey, D., Hogg, D. W., Lang, D., & Goodman, J. 2013, PASP, 125, 306
Gardner, J. P., Brown, T. M., & Ferguson, H. C. 2000, ApJL, 542, L79
Gaté, F., Biteau, J., Batista, R. A., et al. 2017, Proc. ICRC (Busan), 301, 623
Gilmore, R. C., Somerville, R. S., Primack, J. R., & Domínguez, A. 2012, MNRAS, 422, 3189
Goodman, J., & Weare, J. 2010, Communications in Applied Mathematics and Computational Science, 5, 65
Hauser, M. G., Arendt, R. G., Kelsall, T., et al. 1998, ApJ, 508, 25
H.E.S.S. Collaboration, Abdalla, H., Abramowski, A., et al. 2017, A&A, 606, A59
Keenan, R. C., Barger, A. J., Cowie, L. L., & Wang, W.-H. 2010, ApJ, 723, 40
Khaire, V., & Srianand, R. 2018, arXiv:1801.09693
Kneiske, T. M., & Dole, H. 2010, A&A, 515, A19
Magic Collaboration 2019, MNRAS, submitted
Matsuoka, Y., Ienaka, N., Kawara, K., & Oyabu, S. 2011, ApJ, 736, 119
Matsuura, S., Arai, T., Bock, J. J., et al. 2017, ApJ, 839, 7
Mattila, K., Väisänen, P., Lehtinen, K., von Appen-Schnur, G., & Leinert, C. 2017, MNRAS, 470, 2152
Mazin, D., & Raue, M. 2007, A&A, 471, 439
Meyer, M., Horns, D., & Zechlin, H. S. 2010, A&A, 523, A2
Meyer, M., Raue, M., Mazin, D., & Horns, D. 2012, A&A, 542, A59
Raue, M., & Meyer, M. 2012, ApJ, 426, 1097
Stecker, S. W., Scully, S. T., & Malkan, M. A. 2016, ApJ, 827, 6
The Fermi-LAT Collaboration 2018, Sci, 362, 1031
Voyer, E. N., Gardner, J. P., Teplitz, H. I., Siana, B. D., & de Mello, D. F. 2011, ApJ, 736, 80
Xu, C. K., Donas, J., Arnouts, S., et al. 2005, ApJL, 619, L11